

Lateral Photocurrent Method for Directly Measuring the Sheet Resistance of a Junction Partner for a Chalcogenide Light Absorber in a Thin-Film Solar Cell

Choong-Heui Chung[✉]

*Department of Materials Science and Engineering, Hanbat National University, Daejeon 34158,
Republic of Korea*

(Received 20 July 2021; revised 25 January 2022; accepted 1 March 2022; published 21 March 2022)

The purpose of this study is to develop a method for directly measuring the sheet resistance of a junction partner for a chalcogenide light absorber in a thin-film solar cell. The developed method is applied to CdS in a Cu(In, Ga)Se₂ (CIGS) thin-film solar cell as a proof of concept. The suggested method utilizes a combination of the lateral photocurrent flowing along CdS in a custom-designed cell and the current density–voltage curve of a lab-scale CIGS solar cell. By combining an equivalent circuit analysis and a derived approximate equation, a semiempirical formula is proposed for directly measuring the sheet resistance of CdS in the CIGS thin-film solar cell. The semiempirical formula is a function of the basic characteristics (fill factor, short-circuit current density, open-circuit voltage) of the CIGS solar cell, and the linear lateral photocurrent density measured in the custom-designed cell. The proposed semiempirical formula is validated by measuring the sheet resistance of a ZnO:Al thin film in a custom-modified cell. The sheet resistance value agrees well with the sheet resistance value measured by a four-point probe. This method can be easily extended to Cu₂ZnSnS₄, SnS, and Sb₂Se₃ thin-film solar cells, which have very similar device structures to a CIGS thin-film solar cell.

DOI: 10.1103/PhysRevApplied.17.034051

I. INTRODUCTION

To better understand the electronic transport of multilayered electronic devices, characterizing the electrical properties of each functional layer is important. If the growth of a functional layer is influenced by the underlayer, then its electrical properties must be directly characterized in the device. CdS is well known as one of the best *p-n* junction partners for Cu(In, Ga)Se₂ (CIGS) [1–4] and is commonly grown using chemical bath deposition [1–4]. The growth of chemical-bath-deposited CdS is strongly influenced by the underlayer [5–12]. Although CdS is deposited under the same experimental condition, a CdS thin film is deposited on the CIGS surface, but CdS particles are deposited on the glass (Fig. 1). It has been reported that the growth of CdS is also affected by the surface roughness of the substrate [6] and the lattice mismatch between CdS and the substrate [7]. It is even influenced by the composition [8,9] and grain orientation [10–12] at the CIGS surface. Therefore, the electrical properties of CdS must be measured directly in the device.

As mentioned previously, although the growth dependence of chemical-bath-deposited CdS on the underlayer has been reported by several research groups [5–12], a common solution to directly measure the electrical properties of CdS in a CIGS thin-film solar cell has not been reported.

Many solar cells generally use some nonmetallic buffer layer between the active layer and the top electrode to improve their electrical performance. For example, chalcogenide thin-film solar cells, including CIGS [13], Cu₂ZnSnS₄ [14], SnS [15], and Sb₂Se₃ [16] generally use buffer layers such as CdS, ZnS, In₂S₃, or Zn_{1-x}Mg_xO between their light absorber layers and top transparent conducting oxides. MoO_x [17] or bathocuproine [18] buffer for perovskite solar cells, and Ga₂O₃ [19] buffer for cuprous oxide solar cells have been used between the light absorber layers and top electrodes to improve device performances. Therefore, if we develop a method for directly measuring the sheet resistance of CdS, $R_{S(CdS)}$, in a CIGS device, the developed method can be applied to a wider range of solar cells, as well as related diode applications.

This study proposes a method to directly measure the sheet resistance of CdS through a lateral photocurrent method using a paired set of a custom-designed cell and a laboratory-scale CIGS solar cell. The custom-designed cell consists of a planar stack of CdS/CIGS/Mo with a patterned opaque top metal contact [Fig. 2(a)], and the CIGS solar cell is a planar stack of

* choong@hanbat.ac.kr

Published by the American Physical Society under the terms of the [Creative Commons Attribution 4.0 International license](#). Further distribution of this work must maintain attribution to the author(s) and the published article's title, journal citation, and DOI.

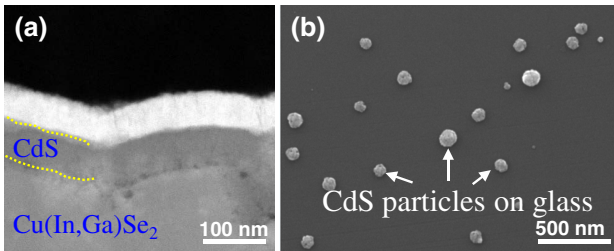


FIG. 1. The growth of chemical-bath-deposited CdS is strongly influenced by the underlayer. (a) Cross-section transmission electron microscope image of CdS grown on the CIGS surface. (b) Plane scanning electron microscope image of CdS grown on glass.

ZnO:Al/iZnO/CdS/CIGS/Mo, where ZnO:Al is Al-doped ZnO and iZnO is intrinsic ZnO [Fig. 2(b)]. The suggested method is based on a combination of the lateral photocurrent (i_{LP}) flowing along CdS in the custom-designed cell and current density–voltage ($J-V$) data of the lab-scale CIGS solar cell. First, analysis of an equivalent circuit for the custom-designed cell provides a numerical relationship between i_{LP} and $R_{S(CdS)}$. Second, mathematical derivation provides an approximate theoretical formula relating i_{LP} and $R_{S(CdS)}$ assuming FF = 100%, where FF is the fill factor of the CIGS solar cell. Finally, a combination of the equivalent circuit analysis and the approximate theoretical formula provides a semiempirical formula relating i_{LP} and $R_{S(CdS)}$, considering the actual FF value.

Highly resistive CdS could cause a loss in FF of CIGS solar cells [20,21]. The resistivity of CdS can have a much greater effect on the performance of the solar cells when we employ a network-type transparent conducting electrode (TCE) to replace sputtered ZnO:Al/iZnO for a CIGS solar cell (Fig. 3). Charge carriers present in the empty space in the network-type TCE laterally travel along the CdS layer to reach the TCE [22,23], which causes resistive

power loss related to $R_{S(CdS)}$ and the size of the empty space (L_{mesh}) of the network-type TCE. Therefore, measuring $R_{S(CdS)}$ under device operating conditions is essential to choose and design the most suitable network-type TCE. Network-type TCEs such as metal nanowires [23–25] and metal meshes [26–28] have been extensively studied to replace sputtered transparent conducting oxides for optoelectronic devices due to their low-cost processing and excellent mechanical flexibility.

II. LATERAL PHOTOCURRENT METHOD

The suggested lateral photocurrent method for measuring $R_{S(CdS)}$ is based on a short-circuited custom-designed cell paired with a lab-scale CIGS solar cell under light illumination (Fig. 2). First, the variations in the current and voltage in the custom-designed cell are described in Sec. II A. Second, a numerical solution for $R_{S(CdS)}$ is shown based on an equivalent circuit analysis for the custom-designed cell in Sec. II B. In Sec. II C, an approximate mathematical formula for $R_{S(CdS)}$ is derived assuming FF = 100% of the CIGS solar cell. Finally, a semiempirical formula considering the actual FF value is introduced by combining the equivalent circuit analysis and the approximate formula in Sec. II D.

A. Custom-designed cell

A cell composed of a planar stack of CdS/CIGS/Mo with a patterned opaque top metal contact is custom-designed [Fig. 2(a)]. Although the bar-shaped top metal contact is not essential in principle, this simple shape is chosen for mathematical convenience. Therefore, for electrodes with other shapes, width (W) in Fig. 2(a) can be simply replaced by the length of the current collecting side of the top metal contact. The length (L) of the custom-designed cell can be any size as long as it is greater than the lateral charge carrier collection length along CdS

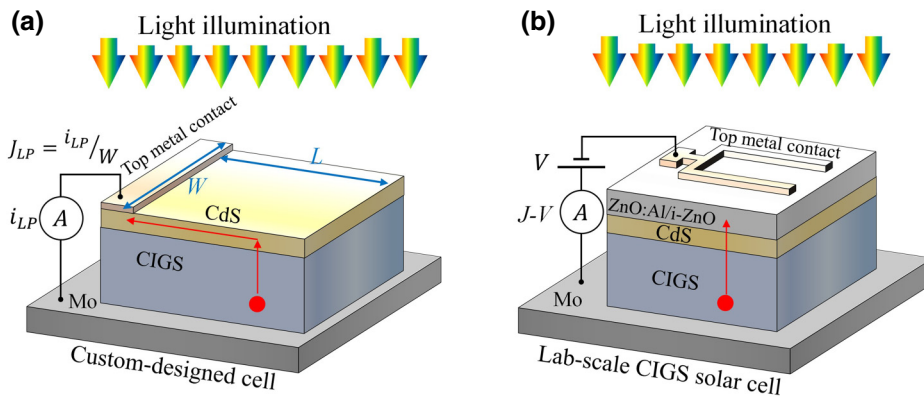


FIG. 2. Illustration of a paired set of two CIGS devices necessary to determine the sheet resistance of CdS. (a) Custom-designed cell with a stack of CdS/CIGS/Mo under light illumination to measure the lateral photocurrent (i_{LP}) flowing along CdS. (b) Lab-scale CIGS solar cell with a standard stack of ZnO:Al/iZnO/CdS/CIGS/Mo under the same light illumination to measure $J-V$ curve.

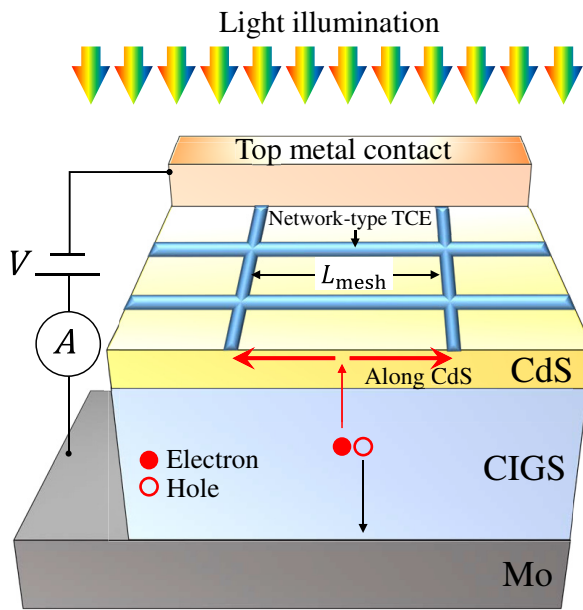


FIG. 3. A schematic of a CIGS solar cell having a network-type TCE as a window layer, where charge carriers present in the empty space in the network-type TCE would horizontally travel along the CdS layer to reach the TCE.

(approximately $25 \mu\text{m}$ in this work). This is because the photocurrent generated farther than the lateral collection length is negligibly small [22]. Please note that there is no ZnO:Al/iZnO on CdS in the custom-designed cell, in contrast to a lab-scale CIGS solar cell with a planar stack of ZnO:Al/iZnO/CdS/CIGS/Mo [Fig. 2(b)].

Let us describe the current flow and voltage variation in the custom-designed cell to lay the foundation for developing the relationship between i_{LP} and $R_{S(CdS)}$. When we shine light on the short-circuited custom-designed cell, electron-hole pairs are generated in the bulk of CIGS, and the electrons vertically travel to reach CdS. Once the electrons reach CdS, they travel horizontally along CdS and are collected by the top metal contact as an external photocurrent [Fig. 4(a)]. The direction of current flow is the reverse to that of electron flow and marked by arrows in Fig. 4(b). The positive direction of current flow is set to be from left to right along CdS and from top to bottom across CIGS [Fig. 4(b)]. The horizontal current flow from the top metal contact along CdS (i_{CdS}) causes a decrease in the voltage at the surface of CdS (V_{CdS}) due to the current times resistance (IR) drop with increasing distance from the top metal contact [Fig. 4(c)]. V_{CdS} corresponds to the voltage difference across CIGS because Mo is grounded. This IR drop causes a forward diode current, whose direction is the reverse of the direction of the photogenerated current [Fig. 4(d)]. V_{CdS} gradually decreases, reaching $-V_{OC}$ at some point, where V_{OC} is the open-circuit voltage for the lab-scale CIGS solar cell. Then, the photogenerated current is canceled out by the diode current, resulting in both a net

current across CIGS (i_{CIGS}) and i_{CdS} being zero. After that, the IR drop along CdS thus no longer occurs even with a further distance from the top metal contact. Therefore, we can divide the custom-designed cell into two regions: zone A of $0 \geq V_{CdS} \geq -V_{OC}$ and zone B of $V_{CdS} = -V_{OC}$. The IR drop along Mo is neglected because the sheet resistance of Mo (about $0.75 \Omega/\text{sq}$ in this work) is much lower than $R_{S(CdS)}$ (estimated to be about $30 \text{ M}\Omega/\text{sq}$ in this work) in this work.

B. Equivalent circuit analysis

An equivalent circuit for a custom-designed cell is constructed based on the variations in the current and voltage in it and characteristic parameters of a lab-scale CIGS solar cell paired with the custom-designed cell. A fabricated solar cell shows $V_{OC} = 711 \text{ mV}$, $J_{SC} = 30.8 \text{ mA/cm}^2$, and $FF = 73.7\%$ [Fig. 5(a)]. Here, two more characteristic parameters V_{max} and ΔV are introduced. V_{max} is defined as the maximum value among the voltage coordinate values of the $J-V$ data between $V = 0$ and $V = V_{OC}$, and ΔV as the voltage interval when we measure the $J-V$ of the CIGS solar cell. Therefore, $V_{max} = 710 \text{ mV}$, and $\Delta V = 10 \text{ mV}$ in this work [Fig. 5(b)].

Figure 6(a) shows the equivalent circuit for zone A of the short-circuited custom-designed cell paired with the above CIGS solar cell under light illumination. Nodes are positioned along CdS from node 0 to node $n+1$. The node voltages are assigned based on the characteristic parameters of the above CIGS solar cell. The voltage at node 0 (V_0) is assigned to be $V_0 = -V_{OC}$. The node voltage at node k (V_k) is assigned to be $V_k = -V_{max} + (k-1)\Delta V$ for $1 \leq k \leq n+1$, where $n = V_{max}/\Delta V$. V_{OC} , V_{max} , and ΔV are then determined to be 0.711 , 0.710 , and 0.01 V from the previous paragraph, and so $V_k = -0.71 + 0.01(k-1)$ for $1 \leq k \leq 72$ in this work. The equivalent circuit consists of $n+1$ microcells. Each microcell has a CIGS micro-solar-cell with an area of $W\Delta x_k$, and a CdS microresistor with a resistance of $R_k [= R_{S(CdS)}(\Delta x_k/W)]$, a length of Δx_k , and a width of W . The current across the CIGS micro-solar-cell from node k to Mo is $i_{CIGSk} = J_{CIGSk}W\Delta x_k$, where J_{CIGSk} is the current density across the CIGS micro-solar-cell connected to node k .

How to obtain $J_{CIGSk} - V_k$ for the CIGS micro-solar-cells is explained in detail as follows: V_k is the voltage at node k positioned at CdS with respect to Mo [Fig. 6(a)]. V of the $J-V$ data of the CIGS solar cell is the voltage at Mo with respect to the top transparent conducting electrode (see Fig. 5). Voltage drop through the top transparent conducting electrode in the lab-scale solar cell is negligible. Therefore, both V_k and V correspond to the voltage difference across CIGS between Mo and CdS while their polarities are opposite. Assuming that the photogenerated current densities in the custom-designed cell and the CIGS solar cell are approximately equal (this assumption

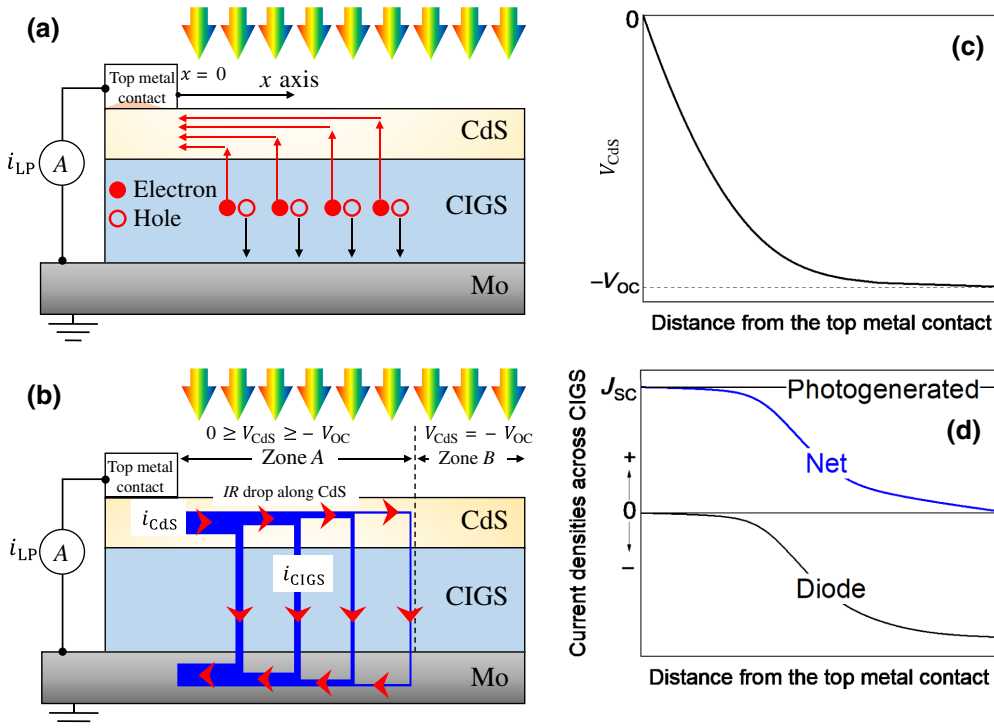


FIG. 4. Illustration of the current flow and voltage variation in a short-circuited custom-designed cell under light illumination. (a) Photogenerated electrons flow across CIGS, and along CdS in a custom-designed cell. (b) Current flows along CdS, and across CIGS in a custom-designed cell. (c) A schematic of V_{CdS} as a function of distance from the top metal contact in linear scale. (d) A schematic of current densities (photogenerated, diode, and net) flowing across CIGS as a function of distance from the top metal contact in a linear scale.

is verified in the Appendix), $J_{\text{CIGS}k} - V_k$ [Fig. 6(b)] can be obtained by reflecting $J-V$ [Fig. 5(a)] of the CIGS solar cell across the current-density axis. Thus, we now have the set of $(V_k, J_{\text{CIGS}k})$ coordinates as follows: $(V_0, J_{\text{CIGS}0}) = (-0.711, 0)$, $(V_1, J_{\text{CIGS}1}) = (-0.71, 0.47)$, $(V_2, J_{\text{CIGS}2}) = (-0.70, 4.73)$, $(V_3, J_{\text{CIGS}3}) = (-0.69, 8.56)$, etc., for the CIGS micro-solar-cells in the equivalent circuit [Fig. 6(c)].

Let us now determine i_{LP} as a function of variable $R_{S(\text{CdS})}$ using the equivalent circuit of Fig. 6(a). We have

the relationships at node k and R_k

$$\begin{aligned} i_k &= i_{k-1} + i_{\text{CIGS}k}, \quad i_{\text{CIGS}k} = J_{\text{CIGS}k} W \Delta x_k, \\ i_k R_k &= \Delta V, \quad \text{and} \quad R_k = R_{S(\text{CdS})} \frac{\Delta x_k}{W}. \end{aligned} \quad (1)$$

Since we assign V_0 to be $-V_{\text{OC}}$, $J_{\text{CIGS}0} = 0$, so $i_0 = i_{\text{CIGS}0} = J_{\text{CIGS}0} W \Delta x_0 = 0$. Solving simultaneous Eq. (1) provides Δx_k and i_k as follows:

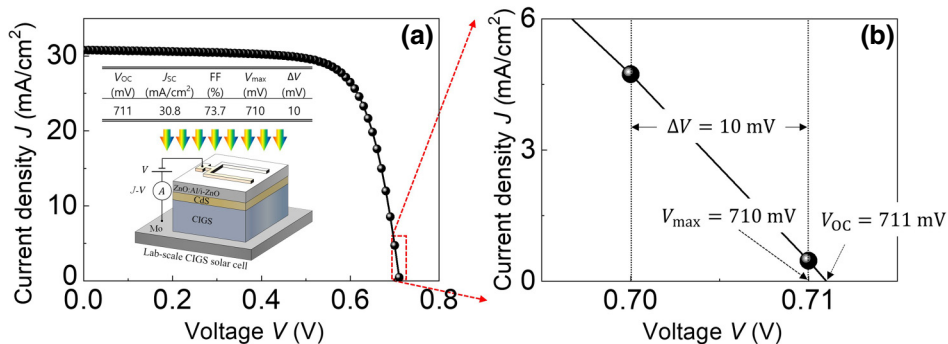


FIG. 5. Measured $J-V$ curve of a fabricated lab-scale CIGS solar cell. The CIGS solar cell shows (a) $V_{\text{OC}} = 711 \text{ mV}$, $J_{\text{SC}} = 30.8 \text{ mA/cm}^2$, and $\text{FF} = 73.7\%$; (b) $V_{\text{max}} = 710 \text{ mV}$, and $\Delta V = 10 \text{ mV}$.

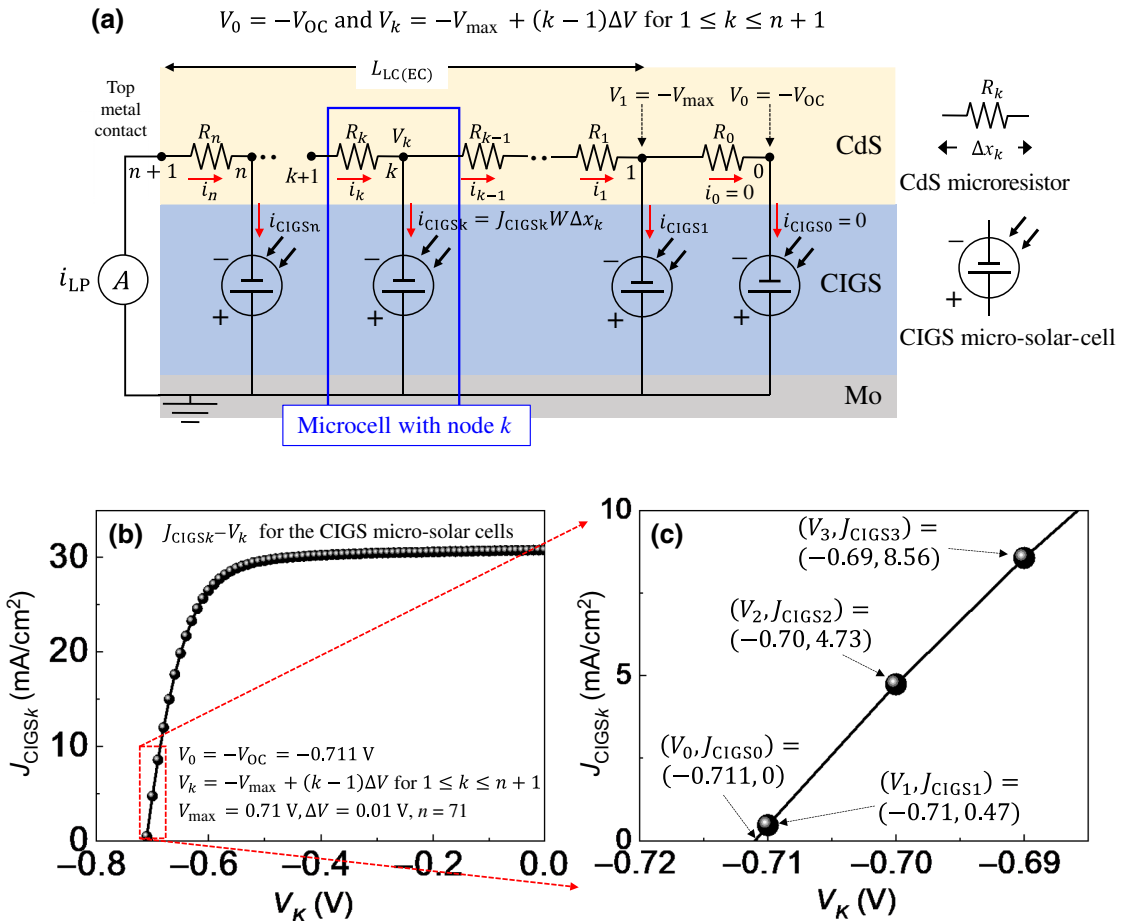


FIG. 6. (a) Equivalent circuit for a short-circuited custom-designed cell under light illumination paired with the CIGS solar cell of Fig. 5. (b) $J_{CIGSk} - V_k$ relationship for the CIGS micro-solar-cells in the equivalent circuit. (c) Several examples of (V_k, J_{CIGSk}) coordinate values for the CIGS micro-solar-cells in the equivalent circuit.

$$\Delta x_k = \frac{-i_{k-1}R_{S(Cds)} + \sqrt{(i_{k-1}R_{S(Cds)})^2 + 4J_{CIGSk}R_{S(Cds)}\Delta VW^2}}{2J_{CIGSk}R_{S(Cds)}W}, \quad (2a)$$

$$i_k = i_{k-1} + J_{CIGSk}W\Delta x_k = i_{k-1} + \frac{-i_{k-1}R_{S(Cds)} + \sqrt{(i_{k-1}R_{S(Cds)})^2 + 4J_{CIGSk}R_{S(Cds)}\Delta VW^2}}{2R_{S(Cds)}}. \quad (2b)$$

i_{LP} ($i_{LP} = i_n$) and $L_{LC(EC)}$ ($= \sum_{k=1}^{k=n} \Delta x_k$) as a function of variable $R_{S(Cds)}$ can be obtained by repeating the calculation using Eqs. (2a) and (2b) from node 1 and R_1 to node n and R_n . $L_{LC(EC)}$ corresponds to the lateral charge carrier collection length along CdS in the custom-designed cell under light illumination. We intuitively know that i_{LP} is linearly proportional to W [see Fig. 2(a)]. Therefore, the relationship between J_{LP} ($= i_{LP}/W$) and $R_{S(Cds)}$

is shown in the following. A flow chart briefly summarizing how to obtain the numerical relationship between $R_{S(Cds)}$, J_{LP} , and $L_{LC(EC)}$ is shown in Fig. 7(a). Figure 7(b) shows the numerical relationship between $R_{S(Cds)}$ and J_{LP} obtained from the equivalent circuit analysis. This numerical $\log_{10}[R_{S(Cds)}] - \log_{10}[J_{LP}]$ relationship shows a slope of -2 , indicating that $R_{S(Cds)}$ is inversely proportional to the square of J_{LP} .

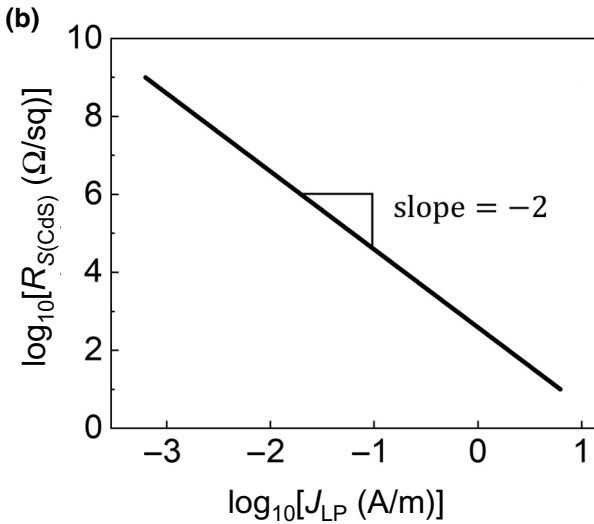
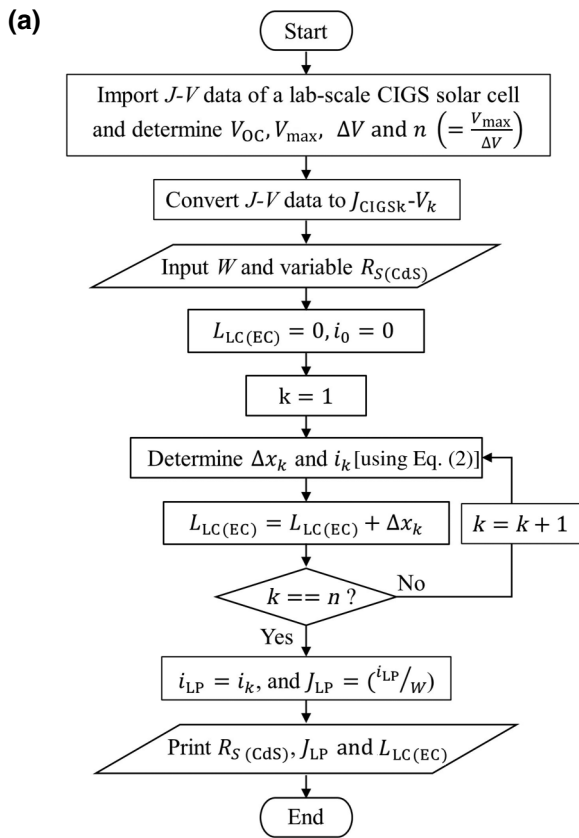


FIG. 7. Analysis of the equivalent circuit of Fig. 6(a). (a) Flow chart showing how to obtain the numerical relationship between $R_{S(\text{CdS})}$, J_{LP} , and $L_{LC(\text{EC})}$. (b) Numerical $\log_{10}[R_{S(\text{CdS})}] - \log_{10}[J_{LP}]$ relationship obtained by the equivalent circuit analysis.

C. Approximate mathematical formula

Although the above equivalent circuit analysis provides a numerical solution for determining $R_{S(\text{CdS})}$, having a mathematical formula relating $R_{S(\text{CdS})}$ to measurable characteristic parameters is more convenient. Here, an

approximate mathematical formula for $R_{S(\text{CdS})}$ is derived based on the change in i_{Cds} and V_{Cds} between x and $x + dx$ in a custom-designed cell [Fig. 8(a)]. J_{CIGS} gradually decreases from J_{SC} to 0 with increasing distance from the top metal contact in the short-circuited custom-designed cell under light illumination [Fig. 8(b)], where J_{CIGS} and J_{SC} are the current density across CIGS in the custom-designed cell and the short-circuit current density of the CIGS solar cell. However, to avoid mathematical complexity in deriving Eq. (9), we assume $J_{\text{CIGS}}(x) = J_{\text{SC}}$ for $0 \leq x \leq L_{\text{LC}(\text{math})}$ and $J_{\text{CIGS}}(x) = 0$ for $x > L_{\text{LC}(\text{math})}$ in the custom-designed cell [Fig. 8(b)]. This assumption corresponds to FF = 100% of the CIGS solar cell paired with the custom-designed cell.

Let us set the position of the front edge of the top metal contact to be $x = 0$ and the position of the boundary between zone A and zone B to be $x = L_{\text{LC}(\text{math})}$. Here, approximate mathematical formula is derived based on the boundary conditions at $x = 0$ and $x = L_{\text{LC}(\text{math})}$ and changes in i_{Cds} and V_{Cds} between x and $x + dx$ [Fig. 8(a)].

We have boundary conditions at $x = 0$ and $x = L_{\text{LC}(\text{math})}$ as follows:

$$i_{\text{Cds}}(x = 0) = i_{LP}, \text{ and } V_{\text{Cds}}(x = 0) = 0, \quad (3a)$$

$$i_{\text{Cds}}(x = L_{\text{LC}(\text{math})}) = 0, \text{ and } V_{\text{Cds}}(x = L_{\text{LC}(\text{math})}) = -V_{\text{OC}}. \quad (3b)$$

The change in i_{Cds} between x and $x + dx$ [$di_{\text{Cds}}(x)$] is equal to $-i_{\text{CIGS}}$. We then have the following relationship because we assume $J_{\text{CIGS}}(x) = J_{\text{SC}}$ for $0 \leq x < L_{\text{LC}(\text{math})}$:

$$di_{\text{Cds}}(x) = -i_{\text{CIGS}}(x) = -J_{\text{CIGS}}(x)Wdx = -J_{\text{SC}}Wdx. \quad (4)$$

Integrating Eq. (4) from $x = 0$ to $x = x$ provides the following equation:

$$i_{\text{Cds}}(x) = i_{LP} - J_{\text{SC}}Wx. \quad (5)$$

Substituting $L_{\text{LC}(\text{math})}$ for x provides $L_{\text{LC}(\text{math})}$ as follows:

$$L_{\text{LC}(\text{math})} = \frac{(i_{LP}/W)}{J_{\text{SC}}} = \frac{J_{LP}}{J_{\text{SC}}}. \quad (6)$$

The change in V_{Cds} between x and $x + dx$ [$dV_{\text{Cds}}(x)$] due to the IR drop along CdS can be expressed as follows:

$$dV_{\text{Cds}}(x) = -i_{\text{Cds}}(x) \frac{R_{S(\text{CdS})}}{W} dx, \quad (7)$$

where $(R_{S(\text{CdS})}/W)dx$ is the resistance along CdS between x and $x + dx$. By substituting $i_{LP} - J_{\text{SC}}Wx$ for $i_{\text{Cds}}(x)$

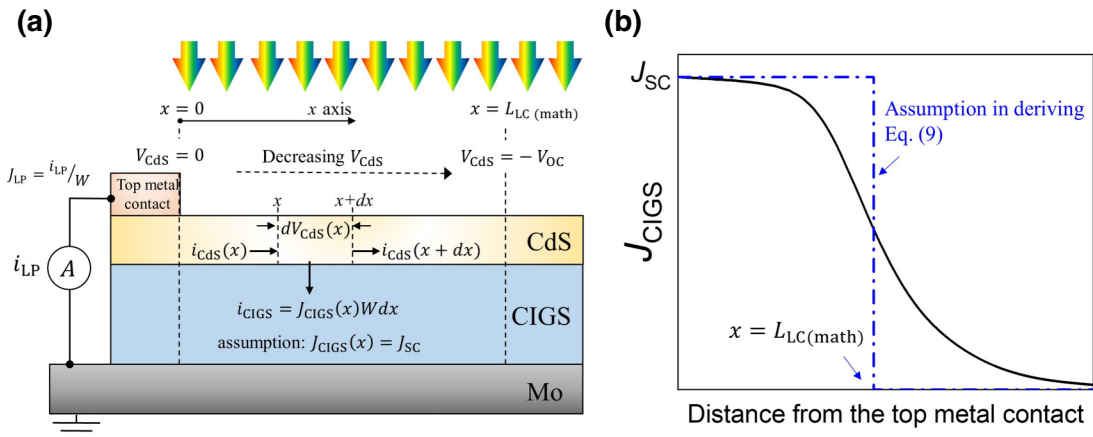


FIG. 8. Illustration of the variation in current and voltage in the short-circuited custom-designed cell under light illumination to derive an approximate mathematical formula Eq. (9). (a) Change in i_{CdS} and V_{CdS} between x and $x+dx$. (b) A schematic sketch of J_{CIGS} as a function of x . Although J_{CIGS} gradually decreases from J_{SC} to 0, we assume $J_{\text{CIGS}}(x) = J_{\text{SC}}$ for $0 \leq x < L_{\text{LC}(\text{math})}$ and $J_{\text{CIGS}}(x) = 0$ for $x \geq L_{\text{LC}(\text{math})}$.

[see Eq. (5)] and integrating Eq. (7) from $x = 0$ to $x = L_{\text{LC}(\text{math})}$, the following equation is obtained:

$$V_{\text{OC}} = J_{\text{LP}} R_{S(\text{CdS})} L_{\text{LC}(\text{math})} - \frac{1}{2} J_{\text{SC}} R_{S(\text{CdS})} L_{\text{LC}(\text{math})}^2. \quad (8)$$

By substituting $J_{\text{LP}}/J_{\text{SC}}$ for $L_{\text{LC}(\text{math})}$ in Eq. (8), we can obtain $R_{S(\text{CdS})}$ as a function of J_{LP} of the custom-designed cell, and J_{SC} and V_{OC} of the CIGS solar cell paired with the custom-designed cell as follows:

$$R_{S(\text{CdS})} = 2 \frac{J_{\text{SC}} V_{\text{OC}}}{J_{\text{LP}}^2}. \quad (9)$$

D. Semiempirical formula

Equation (9) provides a mathematical expression between $R_{S(\text{CdS})}$, J_{SC} , V_{OC} , and J_{LP} , and well explains the slope of -2 in the $\log_{10}[R_{S(\text{CdS})}] - \log_{10}[J_{\text{LP}}]$ plot of Fig. 7(b) generated by the equivalent circuit analysis. However, Eq. (9) has the problem that the FF of a CIGS solar cell paired with a custom-designed cell is assumed to be 100%. Therefore, Eq. (9) can be modified as follows, considering the actual FF value of the CIGS solar cell,

$$R_{S(\text{CdS})} = f(\text{FF}) \times 2 \frac{J_{\text{SC}} V_{\text{OC}}}{J_{\text{LP}}^2}, \quad (10)$$

where $f(\text{FF})$ depends on FF. Therefore, the slope in the plot of $R_{S(\text{CdS})}$ versus $2J_{\text{SC}}V_{\text{OC}}/J_{\text{LP}}^2$ is $f(\text{FF})$.

Sixteen $J-V$ curves of lab-scale CIGS solar cells with a wide range of FF values from 0.45 to 0.78 are used to obtain the $f(\text{FF})$ function [Fig. 9(a)]. We can then have 16 virtual custom-designed cells, each paired with each CIGS solar cell showing one of the 16 $J-V$ curves. The plots of $R_{S(\text{CdS})}$ versus $2J_{\text{SC}}V_{\text{OC}}/J_{\text{LP}}^2$ obtained from the equivalent

circuit analysis for the 16 virtual custom-designed cells are perfectly linear with different slopes [Fig. 9(b)]. To obtain function f (FF), the values of the slopes obtained in Fig. 9(b) are plotted as a function of FF in Fig. 9(c). Linear fitting provides $f(\text{FF}) = 0.63\text{FF} + 0.43$. Therefore, a semiempirical formula for determining $R_{S(\text{CdS})}$ is proposed as follows:

$$R_{S(\text{CdS})} = (0.63\text{FF} + 0.43) \times 2 \frac{J_{\text{SC}} V_{\text{OC}}}{J_{\text{LP}}^2} \text{ for } 0.45 < \text{FF} < 0.78 \quad (11)$$

Please note that semiempirical Eq. (11) is a mathematical expression for the equivalent circuit analysis.

III. APPLICATION TO CIGS DEVICES

A. Fabrication and characterization

A fabricated CIGS solar cell has a standard structure of Al/Ni/ZnO:Al/iZnO/CdS/CIGS/Mo, as depicted in Fig. 2(b). A CIGS light absorber layer ($2 \mu\text{m}$) is deposited onto Mo-coated soda-lime glass substrates by three-stage coevaporation [29], and a CdS buffer (60 nm) is prepared on the CIGS surface by chemical bath deposition based on cadmium sulfate hydrate [5]. A ZnO:Al(450 nm)/iZnO(50 nm) window layer is subsequently deposited onto CdS (60 nm) via radio frequency magnetron sputtering. Finally, the top metal contact Al(850 nm)/Ni(50 nm) is deposited using evaporation through a shadow mask. The active area (approximately 0.42 cm^2) of the CIGS solar cell is defined by mechanical scribing. A custom-designed cell has a structure of Al/Ni/CdS/CIGS/Mo, as depicted in Fig. 2(a), and is fabricated by skipping the deposition of ZnO:Al/iZnO during the fabrication of the lab-scale CIGS solar cell paired with the custom-designed cell.

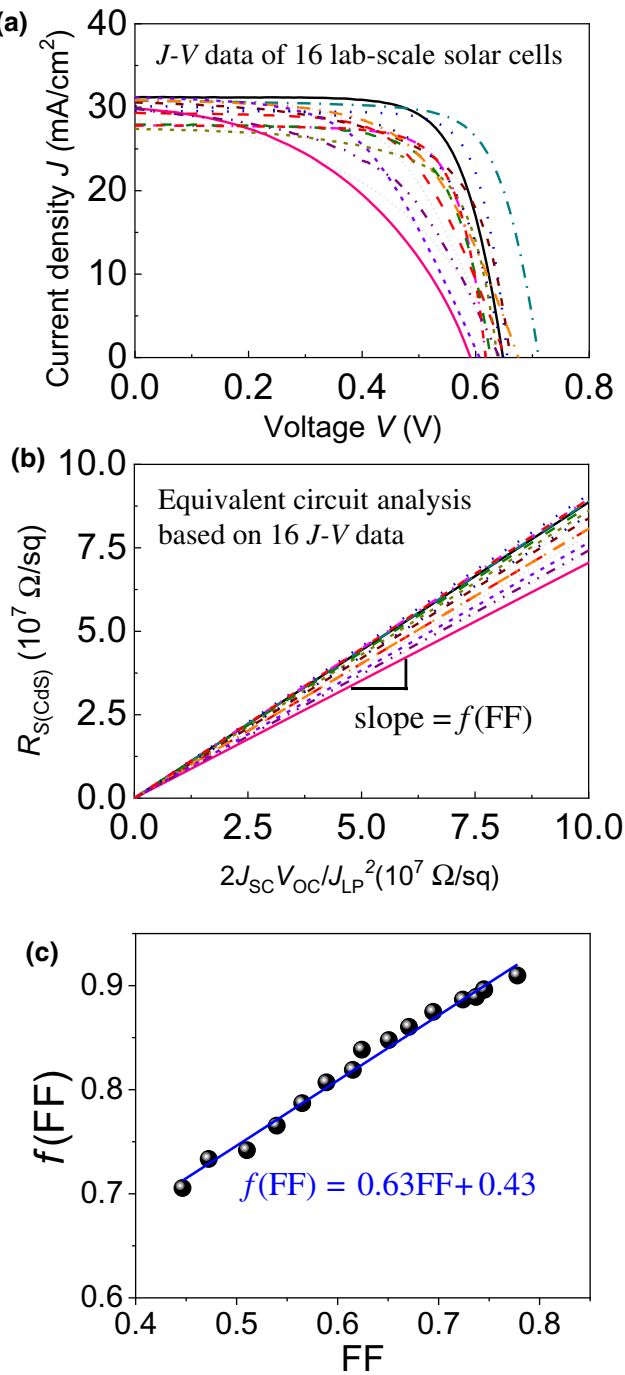


FIG. 9. The process of deriving a semiempirical Eq. (11) for $R_{S(Cds)}$. (a) Sixteen J - V curves of lab-scale CIGS solar cells with a wide range of FF values. (b) Plots of $R_{S(Cds)}$ versus $2J_{SC} V_{OC} / J_{LP}^2$ obtained through the equivalent circuit analysis for the 16 virtual custom-designed cells, each paired with each CIGS solar cell showing one of the 16 J - V curves. (c) Slopes in (b) as a function of FF gives $f(FF) = 0.63FF + 0.43$.

The J - V characteristics of CIGS solar cells are measured using a Keithley 2401 source meter under white-light illumination (100 mW/cm², AM1.5G).

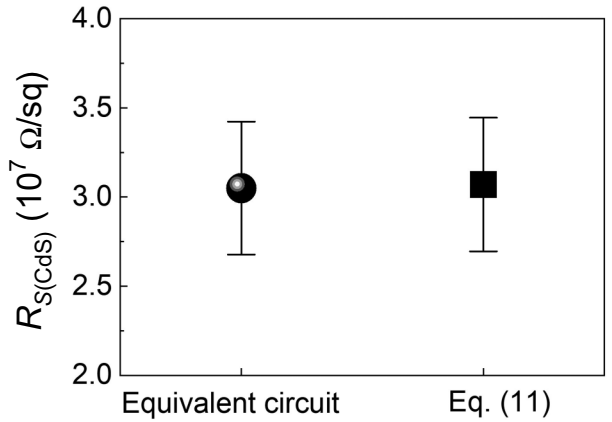


FIG. 10. $R_{S(Cds)}$ determined by equivalent circuit analysis and semiempirical Eq. (11).

generated by a solar simulator (Model 11002 Sun-Lite, Abet Technologies). The lateral photocurrent of the custom-designed cell is measured with a short-circuited Keithley 2401 source meter under white-light illumination (100 mW/cm², AM1.5G).

B. Measuring $R_{S(Cds)}$ in CIGS devices

The fabricated CIGS solar cell shows $V_{OC} = 711$ mV, $J_{SC} = 30.8$ mA/cm², FF = 73.7%, $V_{max} = 710$ mV, and $\Delta V = 10$ mV (Fig. 5). The J_{LP} measured in eight custom-designed cells, fabricated in the same batch as the CIGS solar cell, are summarized in Table I. $J_{LP} = 3.59 \times 10^{-3} \pm 2.16 \times 10^{-4}$ A/m (average \pm s.d.). $R_{S(Cds)}$ is thus determined to be 30.5 ± 3.7 M Ω/sq and 30.7 ± 3.8 M Ω/sq by the equivalent circuit analysis and semiempirical Eq. (11), respectively (Fig. 10). Since the semiempirical Eq. (11) is a just a mathematical expression for the equivalent circuit analysis, both provide almost the same value. Since $L_{LC(EC)}$ is estimated to be approximately 25 μm and the charge carrier collection length in CIGS is known to be approximately 2 μm [30–32], the photocurrent is captured along CdS in the custom-designed cell as previously described.

C. Validation of the proposed method

To validate the lateral photocurrent method as a tool to measure $R_{S(Cds)}$ in CIGS devices, the method is applied to determine the sheet resistance of a sputtered ZnO:Al thin film using the modified custom-designed cell with a structure of ZnO:Al/iZnO/CdS/CIGS/Mo of Fig. 11(a) paired with the fabricated CIGS solar cell. The photocurrent flows along the ZnO:Al film instead of CdS in the modified custom-designed cell because its sheet resistance ($R_{S(ZnO:Al)} \approx 26 \Omega/\text{sq}$) is much lower than $R_{S(Cds)} \approx 30$ M Ω/sq . Therefore, the lateral photocurrent method provides $R_{S(ZnO:Al)}$, not $R_{S(Cds)}$, in the modified custom-designed cell. In this case, the length (L)

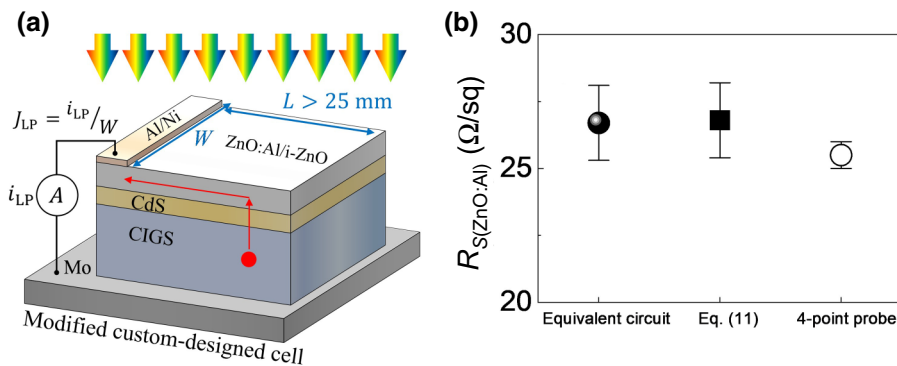


FIG. 11. Validation of the suggested lateral photocurrent method. (a) Modified custom-designed cell to measure $R_{S(\text{ZnO:Al})}$. (b) $R_{S(\text{ZnO:Al})}$ values determined by both equivalent circuit analysis and semiempirical Eq. (11) are very similar to $R_{S(\text{ZnO:Al})}$ values measured by a four-point probe.

of the modified custom-designed cell is kept longer than 25 mm because $L_{LC(EC)}$ is estimated to be approximately 25 mm. The measured J_{LP} values for the modified custom-designed cells are summarized in Table II, and are 3.82 ± 0.10 A/m (average \pm s.d.). $R_{S(\text{ZnO:Al})}$ is then determined to be 26.7 ± 1.4 Ω/sq and 26.8 ± 1.4 Ω/sq by the equivalent circuit analysis and semiempirical Eq. (11), respectively [Fig. 11(b)]. These values are very similar to $R_{S(\text{ZnO:Al})} = 25.5 \pm 0.5$ Ω/sq measured by a four-point probe.

IV. SUMMARY

In summary, a lateral photocurrent method is developed to directly measure the sheet resistance of CdS using a paired set of a custom-designed cell and a lab-scale CIGS solar cell. The equivalent circuit analysis for the short-circuited custom-designed cell under light illumination provides a numerical relationship between $R_{S(\text{CdS})}$ and

J_{LP} . An approximate mathematical formula derived for the custom-designed cell relates $R_{S(\text{CdS})}$ with J_{SC} , V_{OC} , and J_{LP} assuming FF = 100% of the CIGS solar cell. The semiempirical formula of $R_{S(\text{CdS})} = (0.63\text{FF} + 0.43) \times 2J_{SC}V_{OC}/J_{LP}^2$, considering the actual FF value of the CIGS solar cell is proposed by combining the equivalent circuit analysis and the approximate mathematical formula. The sheet resistance of CdS (60 nm) is measured to be approximately 30 MΩ/sq, which corresponds to an electrical resistivity of 1.8×10^2 Ωcm. The semiempirical formula is validated by precisely measuring the sheet resistance of a ZnO:Al thin film in a modified custom-designed cell. This method can be easily applied to other chalcogenide thin-film solar cells such as $\text{Cu}_2\text{ZnSnS}_4$, SnS, and Sb_2Se_3 thin-film solar cells, which have similar device structures and material processes to a CIGS thin-film solar cell.

The data that support the findings of this study are available from the corresponding author upon reasonable request.

TABLE I. Measured J_{LP} values in the eight custom-designed cells, $L_{LC(EC)}$ values determined by the equivalent circuit analysis, and $R_{S(\text{CdS})}$ determined by the equivalent circuit analysis and semiempirical Eq. (11).

Custom-designed cell number	Measured J_{LP} (A/m)	Equivalent circuit analysis		$R_{S(\text{CdS})}$ (Ω/sq)	$R_{S(\text{CdS})}$ (Ω/sq)
		$L_{LC(EC)}$ (μm)	$R_{S(\text{CdS})}$ (Ω/sq)		
1	3.65×10^{-3}	25.2	2.92×10^7	2.94×10^7	
2	3.88×10^{-3}	26.7	2.59×10^7	2.60×10^7	
3	3.79×10^{-3}	26.1	2.71×10^7	2.73×10^7	
4	3.29×10^{-3}	22.7	3.59×10^7	3.62×10^7	
5	3.47×10^{-3}	23.9	3.23×10^7	3.25×10^7	
6	3.62×10^{-3}	24.9	2.97×10^7	2.99×10^7	
7	3.31×10^{-3}	22.8	3.55×10^7	3.58×10^7	
8	3.71×10^{-3}	25.6	2.83×10^7	2.85×10^7	
Average	3.59×10^{-3}	24.7	3.05×10^7	3.07×10^7	
s.d.	2.16×10^{-4}	1.5	3.73×10^6	3.78×10^6	

TABLE II. Measured J_{LP} values in the eight modified custom-designed cells, and $R_{S(\text{ZnO:Al})}$ determined by both the equivalent circuit analysis and semiempirical Eq. (11) are very similar to $R_{S(\text{ZnO:Al})}$ measured by a four-point probe, validating the suggested lateral photocurrent method.

Modified Custom- designed cell number	$R_{S(\text{ZnO:Al})} (\Omega/\text{sq})$		
	Measured J_{LP} (A/m)	Equivalent circuit	Semiempirical Eq. (11)
1	3.90	25.6	25.8
2	3.68	28.8	28.9
3	3.78	27.2	27.4
4	3.96	24.8	25.0
5	3.91	25.5	25.6
6	3.73	28.0	28.2
7	3.84	26.4	26.6
8	3.79	27.1	27.3
Average	3.82	26.7	26.8
s.d.	0.10	1.4	1.4

ACKNOWLEDGMENTS

This research was supported by the research fund of Hanbat National University in 2020 and the Basic Science Research Program through the National Research Foundation of Korea (NRF) funded by the Ministry of Science and ICT (Grant No. NRF-2021R1A2C1005815). The author would like to acknowledge the photovoltaic research department at the Korea Institute of Energy Research for providing CdS/CIGS/Mo samples.

C.-H.C. designed the research, performed experiments and analysis, and wrote the paper.

The author declares no competing financial interests.

APPENDIX

In the main text, we obtain $J_{\text{CIGS}_k} - V_k$ for the CIGS micro-solar cells by reflecting $J-V$ of the CIGS solar cell across the current-density axis and assuming that the photogeneration current densities in the custom-designed cell and the CIGS solar cell paired with the custom-designed cell are approximately equal. This assumption is verified in the following.

The difference in the photogeneration current density between the custom-designed cell and the CIGS solar cell is due to the different amounts of optical loss in the two devices. In a custom-designed cell, optical losses include reflection of incident light off the device surface and absorption by CdS [Fig. 12(a)]. In a CIGS solar cell, optical losses include reflection of incident light off the device surface, and absorption by ZnO:Al/iZnO and CdS. [Figure 12(b)]. The reflectance spectra of both devices are shown in Fig. 12(c). The absorbance (A) by ZnO:Al/iZnO is obtained using the

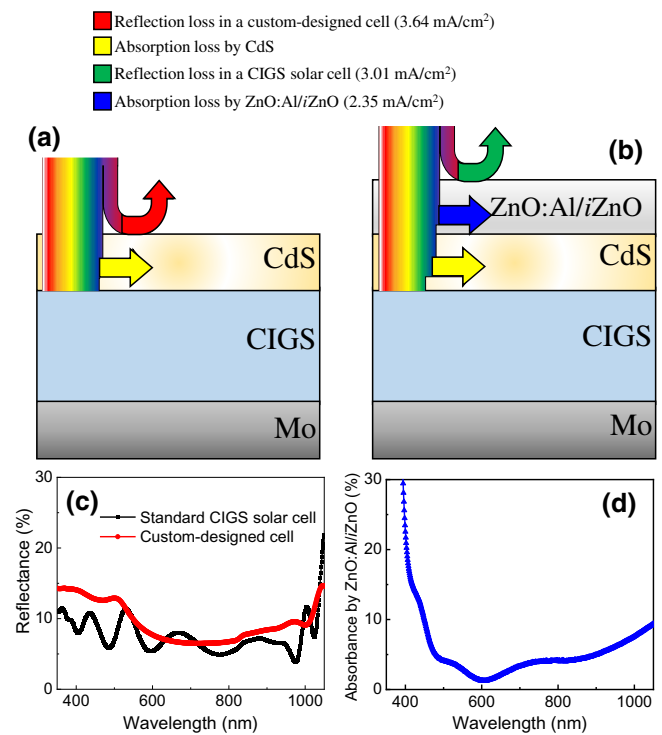


FIG. 12. (a) Optical loss in a custom-designed cell. (b) Optical loss in a CIGS solar cell paired with the custom-designed cell. (c) Reflectance spectra of the two devices. (d) The absorption spectrum by ZnO:Al/iZnO.

formula $A = 1 - R - T$, where reflectance (R) and transmittance (T) are measured for ZnO:Al/iZnO prepared on glass [Fig. 12(d)]. Optical losses can be estimated by integrating the reflectance and absorption spectra multiplied by the light spectrum of AM1.5G. The absorption loss by CdS should be equal on both devices. The reflection loss in the custom-designed cell is estimated to be 3.64 mA/cm^2 . The reflection loss in the CIGS solar cell and the absorption loss by ZnO:Al/iZnO are estimated to be 3.01 and 2.35 mA/cm^2 , respectively. The difference in the optical losses between the two devices is thus estimated to be 1.72 mA/cm^2 . Considering the short-circuit current density (30.8 mA/cm^2) of the CIGS solar cell, the difference in optical losses between the two devices is approximately 5% of the short-circuit current density. Therefore, it should be acceptable to assume that the photogeneration current densities in the custom-designed cell and the CIGS solar cell are approximately equal.

- [1] K. S. Cho, J. Jang, J.-H. Park, D.-K. Lee, S. Song, K. Kim, Y.-J. Eo, J. H. Yun, J. Gwak, and C.-H. Chung, Optimal CdS buffer thickness to form high-quality CdS/Cu(In, Ga)Se₂ junctions in solar cells without plasma damage and shunt paths, *ACS Omega* **5**, 23983 (2020).

- [2] T. Nakada and A. Kunioka, Direct evidence of Cd diffusion into Cu(In, Ga)Se₂ thin films during chemical-bath deposition process of CdS films, *Appl. Phys. Lett.* **74**, 2444 (1999).
- [3] M. Krause, A. Nikolaeva, M. Maiberg, P. Jackson, D. Hariskos, W. Witte, J. A. Márquez, S. Levchenko, T. Unold, R. Scheer, and D. Abour-Ras, Microscopic origins of performance losses in highly efficient Cu(In, Ga)Se₂ thin-film solar cells, *Nat. Commun.* **11**, 1 (2020).
- [4] M. A. Contreras, M. J. Romero, B. To, F. Hasoon, R. Noufi, S. Ward, and K. Ramanathan, Optimization of CBD CdS process in high-efficiency Cu(In, Ga)Se₂-based solar cells, *Thin Solid Films* **403**, 204 (2002).
- [5] S. Lee, E. S. Lee, T. Y. Kim, J. S. Cho, Y. J. Eo, J. H. Yun, and A. Cho, Effect of annealing treatment on CdS/CIGS thin film solar cells depending on different CdS deposition temperatures, *Sol. Energy Mater. Sol. Cells* **141**, 299 (2015).
- [6] D. Bhattacharyya and M. Carter, Effect of substrate on the structural and optical properties of chemical-bath-deposited CdS films, *Thin Solid Films* **288**, 176 (1996).
- [7] A. Oliva, R. Castro-Rodríguez, O. Ceh, P. Bartolo-Perez, F. Caballero-Briones, and V. Sosa, First stages of growth of CdS films on different substrates, *Appl. Surf. Sci.* **148**, 42 (1999).
- [8] T. Kodalle, L. Choubrac, L. Arzel, R. Schlatmann, N. Barreau, and C. A. Kaufmann, Effects of KF and RbF post deposition treatments on the growth of the CdS buffer layer on CIGS thin films - a comparative study, *Sol. Energy Mater. Sol. Cells* **200**, 109997 (2019).
- [9] A. Chirilă, P. Reinhard, F. Pianezzi, P. Bloesch, A. R. Uhl, C. Fella, L. Kranz, D. Keller, C. Gretener, H. Hagendorfer, D. Jaeger, R. Erni, S. Nishiwaki, S. Buecheler, and A. N. Tiwari, Potassium-Induced surface modification of Cu(In, Ga)Se₂ thin films for high-efficiency solar cells, *Nat. Mater.* **12**, 1107 (2013).
- [10] W. Witte, D. Abou-Ras, and D. Hariskos, Chemical bath deposition of Zn(O, S) and CdS buffers: Influence of Cu(In, Ga)Se₂ grain orientation, *Appl. Phys. Lett.* **102**, 051607 (2013).
- [11] W. Witte, D. Abou-Ras, and D. Hariskos, Improved growth of solution-deposited thin films on polycrystalline Cu(In, Ga)Se₂, *Phys. Status Solidi RRL* **10**, 300 (2016).
- [12] T. M. Friedlmeier, P. Jackson, A. Bauer, D. Hariskos, O. Kiowski, R. Wuerz, and M. Powalla, Improved photocurrent in Cu(In, Ga)Se₂ solar cells: From 20.8% to 21.7% efficiency with CdS buffer and 21.0% Cd-free, *IEEE J. Photovoltaics* **5**, 1487 (2015).
- [13] N. Naghavi, D. Abou-Ras, N. Allsop, N. Barreau, S. Bücheler, A. Ennaoui, C. H. Fischer, C. Guillen, D. Hariskos, J. Herrero, R. Klenk, K. Kushiya, D. Lincot, R. Menner, T. Nakada, C. Platzer-Björkman, S. Spiering, A. N. Tiwari, and T. Törndahl, Buffer layers and transparent conducting oxides for chalcopyrite Cu(In, Ga)(S, Se)₂ based thin film photovoltaics: Present status and current developments, *Prog. Photovoltaics* **18**, 411 (2010).
- [14] K.-J. Yang, S. Kim, S.-Y. Kim, K. Ahn, D.-H. Son, S.-H. Kim, S.-J. Lee, Y.-I. Kim, S.-N. Park, S.-J. Sung, D.-H. Kim, T. Enkhbat, J. Kim, C.-W. Jeon, and J.-K. Kang, Flexible Cu₂ZnSn(S, Se)₄ solar cells with over 10% efficiency and methods of enlarging the cell area, *Nat. Commun.* **10**, 1 (2019).
- [15] D. Lim, H. Suh, M. Suryawanshi, G. Y. Song, J. Y. Cho, J. H. Kim, J. H. Jang, C. W. Jeon, A. Cho, S. Ahn, and J. Heo, Kinetically controlled growth of phase-pure SnS absorbers for thin film solar cells: Achieving efficiency near 3% with long-term stability using an SnS/CdS heterojunction, *Adv. Energy Mater.* **8**, 1702605 (2018).
- [16] X. Wen, C. Chen, S. Lu, K. Li, R. Kondrotas, Y. Zhao, W. Chen, L. Gao, C. Wang, J. Zhang, G. Niu, and J. Tang, Vapor transport deposition of antimony selenide thin film solar cells with 7.6% efficiency, *Nat. Commun.* **9**, 1 (2018).
- [17] C. Liu, W. Li, J. Chen, J. Fan, Y. Mai, and R. E. Schropp, Ultra-thin MoO_x as cathode buffer layer for the improvement of all-inorganic CsPbIBr₂ perovskite solar cells, *Nano Energy* **41**, 75 (2017).
- [18] N. Shibayama, H. Kanda, T. W. Kim, H. Segawa, and S. Ito, Design of BCP buffer layer for inverted perovskite solar cells using ideal factor, *APL Mater.* **7**, 031117 (2019).
- [19] Y. S. Lee, D. Chua, R. E. Brandt, S. C. Siah, J. V. Li, J. P. Mailoa, S. W. Lee, R. G. Gordon, and T. Buonassisi, Atomic layer deposited gallium oxide buffer layer enables 1.2 V open-circuit voltage in cuprous oxide solar cells, *Adv. Mater.* **26**, 4704 (2014).
- [20] I. Eisgruber, J. Granata, J. Sites, J. Hou, and J. Kessler, Blue-photon modification of nonstandard diode barrier in CuInSe₂ solar cells, *Sol. Energy Mater. Sol. Cells* **53**, 367 (1998).
- [21] I. Khatri, K. Shudo, J. Matsuura, M. Sugiyama, and T. Nakada, Impact of heat-light soaking on potassium fluoride treated CIGS solar cells with CdS buffer layer, *Prog. Photovoltaics* **26**, 171 (2018).
- [22] S. Lee, J. Jang, K. S. Cho, Y.-J. Oh, K.-H. Hong, S. Song, K. Kim, Y.-J. Eo, J. H. Yun, J. Gwak, and C.-H. Chung, Determination of the lateral collection length of charge carriers for silver-nanowire-electrode-based Cu(In, Ga)Se₂ thin-film solar cells, *Sol. Energy* **180**, 519 (2019).
- [23] S. Lee, J. S. Lee, J. Jang, K.-H. Hong, D.-K. Lee, S. Song, K. Kim, Y.-J. Eo, J. H. Yun, J. Gwak and, and C.-H. Chung, Robust nanoscale contact of silver nanowire electrodes to semiconductors to achieve high performance chalcogenide thin film solar cells, *Nano Energy* **53**, 675 (2018).
- [24] S. Lee, J. Jang, T. Park, Y. M. Park, J. S. Park, Y.-K. Kim, H.-K. Lee, E.-C. Jeon, D.-K. Lee, B. Ahn, and C.-H. Chung, Electrodeposited silver nanowire transparent conducting electrodes for thin-film solar cells, *ACS Appl. Mater. Interfaces* **12**, 6169 (2020).
- [25] P.-C. Hsu, S. Wang, H. Wu, V. K. Narasimhan, D. Kong, H. R. Lee, and Y. Cui, Performance enhancement of metal nanowire transparent conducting electrodes by mesoscale metal wires, *Nat. Commun.* **4**, 1 (2013).
- [26] C. F. Guo, T. Sun, Q. Liu, Z. Suo, and Z. Ren, Highly stretchable and transparent nanomesh electrodes made by grain boundary lithography, *Nat. Commun.* **5**, 1 (2014).
- [27] X. Lu, Y. Zhang, and Z. Zheng, Metal-based flexible transparent electrodes: Challenges and recent advances, *Adv. Electron. Mater.* **7**, 2001121 (2021).

- [28] H. B. Lee, W.-Y. Jin, M. M. Ovhal, N. Kumar, and J.-W. Kang, Flexible transparent conducting electrodes based on metal meshes for organic optoelectronic device applications: A review, *J. Mater. Chem. C* **7**, 1087 (2019).
- [29] S. Lee, K. S. Cho, S. Song, K. Kim, Y.-J. Eo, J. H. Yun, J. Gwak, and C.-H. Chung, Fabrication of robust nanoscale contact between a silver nanowire electrode and CdS buffer layer in Cu(In,Ga)Se₂ thin-film solar cells, *J. Visualized Exp.* **149**, e59909 (2019).
- [30] C.-H. Chung, Method to Determine the Recombination Characteristics of Minority Carriers in Graded-Band-gap Solar Cells, *Phys. Rev. Appl.* **12**, 024060 (2019).
- [31] R. Scheer, M. Wilhelm, H. Lewerenz, H. Schock, and L. Stolt, Determination of charge carrier collecting regions in chalcopyrite heterojunction solar cells by electron-beam-induced current measurements, *Sol. Energy Mater. Sol. Cells* **49**, 299 (1997).
- [32] R. Scheer, C. Knieper, and L. Stolt, Depth dependent collection functions in thin film chalcopyrite solar cells, *Appl. Phys. Lett.* **67**, 3007 (1995).